Egypt. J. Chem. **Vol. 68,** SI: Z. M. Nofal, pp. 77 – 90 (2025)

Egyptian Journal of Chemistry

http://ejchem.journals.ekb.eg/

Advanced Chemical Analysis of Combustion Enhancement in Compressed Natural Gas-Air Flames using Low-Emission System

Mostafa M. Abdel Aziz[a]*, Hatem Kayeda[b], Tharwat W. Abou-Arab[b], Abdelmaged H. Ibrahim[b]

[a]*Mechanical Power Engineering Department, Institute of Aviation Engineering and Technology, Giza 12658, Egypt*

[b]*Mechanical Power Engineering Department, Faculty of Engineering, Cairo University, Giza 12613, Egypt*

Abstract

Compressed Natural Gas (CNG), predominantly composed of methane (CH_4) with minor constituents of higher hydrocarbons and inert gases, is renowned for its clean-burning properties due to its favorable hydrogen-to-carbon ratio. However, under ultra-lean conditions, achieving stable and efficient combustion is chemically challenging because of limited radical formation and suboptimal reaction kinetics. This study presents an in-depth chemical analysis of CNG-Air combustion using an innovative dual-stream burner design. The system integrates an annular pre-mixed CNG-Air stream with a centrally injected diffusion stream of pure CNG, a configuration that alters the local chemical environment and reaction pathways. By varying the diffusion ratio and adjusting the fuel flow rates at different overall equivalence ratios, the study revealed notable chemical and operational enhancements. At a 15% diffusion ratio, the upper limit of the equivalence ratio increased to $\varphi = 1.328$ by achieving an increase of 11% compared to a configuration without central diffusion. Conversely, a 5% diffusion ratio resulted in a dramatic decrease to $\varphi = 0.039$ and a percentage decrease up to 91.5% in the lower equivalence limit. These chemical modifications enhance the lower limits due to the presence of sufficient oxygen for improved chemical reactions, effectively broadening the operability range of ultra-lean combustors. Computational results indicate that the minimum axial temperature and minimum CO_2 concentration were achieved at a 15% diffusion ratio with a recorded decrease of 21.86% and 26.59%, respectively, compared to a 0% diffusion ratio. This is explained by the fact that at greater equivalence ratio values, there is less oxygen available for combustion. However, at a 5% diffusion ratio, the minimum axial temperature and minimum CO_2 concentration were recorded a decrease of 14.75% and 16.89%, respectively, compared to a 0% diffusion ratio. Environmentally, these improvements lead to significantly lower fuel consumption, lower maximum temperature and reduced emissions of greenhouse gases and nitrogen oxides, paving the way for cleaner and more sustainable combustion technologies.

Keywords: CNG combustion; Low-emission combustion; Computational fluid dynamics (CFD); No_x emissions control; Chemical kinetics

Nomenclature and abbreviations

CNG	Compressed natural gas	C_p	Specific heat
φ	Equivalence ratio	N	Total number of species
R_e	Rynolds number of oxidizer	R_o	Universal gas constant
M_f	Fuel mass flow rate	μ	Dynamic viscosity
L	Duct length measured from the mixing point up to the burner tip	λ	Thermal conductivity
L/D	Premixing ratio	g_x	Gravitational acceleration in x direction
D	Burner outer diameter	ω_i	Production rate
D_c	Confinement outer diameter	h_i	Enthalpy
T	Temperature	Y_i	Mass fraction
P	Dynamic pressure	D_i	Mass diffusion coefficient
ρ	Density	M_i	Molecular weight of species i
$\vec{u}$= (u,v)	Velocity vector	D_{ti}	Thermo-diffusion coefficient

1. Introduction

Global warming and rising air pollution levels are the results of an enormous increase in energy consumption carried on by population growth and fast industrial development. There are still several barriers to the worldwide transition to clean, renewable energy, including the expense of implementation in comparison to traditional fossil fuels and the availability of advanced, dependable technologies. Manufacturers of gas turbines created novel combustion strategies for clean power production in gas turbines as a result of the goal of keeping global warming to 2°C and the rising pressure of stringent emissions laws [1]. Ensuring proper combustion conditions and optimizing flame stability are essential strategies for reducing emissions in various combustion systems. The stability and emissions characteristics of various flame types (diffusion and

*Corresponding author e-mail: m.mabdelaziz@iaet.edu.eg; (**Mostafa M. Abdel Aziz**).
Received date 06 March 2025; Revised date 31 March 2025; Accepted date 15 April 2025
DOI: 10.21608/EJCHEM.2025.365932.11405
©2025 National Information and Documentation Center (NIDOC)

partially-premixed) vary, and changing the flame mode can cause significant variations in both the stability and emissions produced. The current burner mixes both flame modes toward reduced emissions under a large operability range [2-3].

Because of their excellent stability behavior under a variety of loading conditions, non-premixed flames have been utilized in gas turbines to generate electricity [4-6]. Nevertheless, these flames produce stoichiometric and near-stoichiometric combustion zones inside the combustor, which leads to the creation of hot regions inside the combustor that increase NOx emissions [7]. Since the reactants are premixed upstream of the combustor, changing from a non-premixed to a premixed combustion mode avoids the formation of stoichiometric combustion zones inside the combustor. When this occurs, the temperature drops, which lowers NOx emissions [8]. But mixing the reactants upstream of the combustor causes the flow field to fluctuate, which then interacts with the pressure field to cause several types of combustion instabilities that negatively impact the operation [9-11].

The fuel flexibility strategy might be a way to improve the overall combustion and emissions characteristics while controlling instabilities related to the premixed mode of combustion. Additionally, oxidizer flexibility can be very important in reducing emissions from gas turbines [12-14].

Natural gas is considered one of the most popular and favored fuels that have been utilized to operate gas turbines over the past three decades since it produces less pollution than other liquid or gaseous fuels designed to prevent global warming. [15-24]. According to Jaramillo et al. [25], natural gas emits 15% less CO2 than crude oil and 40% less than coal. Pretreatment, process adjustments, combustion modification, and post treatment are some of the numerous well-established techniques for reducing and managing NOx emissions. According to several recent research, one of the most promising ways to significantly decrease NOx emissions is to use the partially or fully premixed flame approach. [26-28]. Seiser et al. [29] looked into the flammability and extinction limits of laminar partially-premixed flames, while considering the arrangement of the counter-flow across a range of partial premixing. They found that as the amount of premixing is increased, the flame temperature decreases. Sayangdev and Aggarwal [30] stated that one of the main strategies for lowering NOx and particle emissions from fires is partial premixing. Studies by Tyliszczaketal [31], Nemitallah et al. [32], and Taamallah et al. [33], among others, examined the use of numerical combustion models to forecast stability and emission characteristics in gas turbines. Park et al. [34] examined the impact of hydrogen enrichment by statistically analyzing the whirling premixed methane-air flames in a cuboid combustor. They discovered that diffusion and convection contributions dominate both the local and global flame structures. Lean-premixed hydrogen-enriched methane-air flames were examined by Guo et al. [35]. When hydrogen was added, they observed that the flame brush attachment changed from being comparatively weak to strong.

According to the previously presented studies, the partially-premixed combustion method is one of the most widely used clean burning strategies. This is especially true when using CNG-Air flames, which are thought to be one of the most popular fuels used to power gas turbines and produce less pollution than other liquid or gaseous fuels intended to reduce global warming. However, neither the chemical and thermal structure of the ultra-lean premixed flame nor the instabilities of partially-premixed combustion under ultra-lean conditions were examined in the subjective pattern of the earlier studies.

The current study aims to experimentally investigate the impact of adopting the secondary central diffusion stream with different ratios, namely 0, 5, 10 and 15%, respectively to the primary annular partially-premixed stream aiming to increasing the flame stability and flammability while reducing the emissions at ultra-lean condition. Numerically, the chemical and thermal structure of the CNG-Air partially-premixed flame has been studied to investigate the species transport mechanism for major, minor, and emission chemical concentrations. The current results illustrate the lower and upper flammability limits and analyze the overall visual flame shapes and colors, while achieving a larger operability range of CNG-Air flames, leading to a direct improvement in the efficiency of combustion and emissions reduction.

2. Experimental setup

2.1. The combustor and its instrumentation

The properties of dual diffusion/partially-premixed flames with varying diffusion ratios were examined in the current study for the combustion of CNG in air. The combustor consists of two coaxial streams, a primary annular premixed stream and a secondary central diffusion stream. A perforated plate burner is used to stabilize the premixed flame, while the central diffusion flame was inserted as a central stream with fuel percentages of the diffusion flame to that in the partial premixed mode is 0, 5, 10, and 15%, respectively. Fig.1 displays the schematic diagram for the experimental CNG-Air combustion tests. The exhaust portion, confinement, burner, and gas lines are all depicted in the diagram.

Rotameters were used to measure the volumetric flow rate of all streams, with pressure gages and thermocouples to measure the pressures and temperatures of each stream fed to the burner as per specifications mentioned in Table1. A control needle valve and pressure regulator valve were located on each gas supply line to control the gas flow rate. Two identical pipes, each measuring 3.5 meters in length and 7 mm in inner diameter, are used to supply both gasses to the burner.

The combustion air is supplied by a reciprocating compressor with a 0.5 m3 storage tank. The CNG fuel line is supplied from a commercial CNG bottle (85% CH_4, 9% C_2H_6, 3% C_3H_8, 2.4% CO_2 and 0.6% N_2 by volume; 200 bar) was introduced to the burner through two lines one for the primary annular premixed flame and another for the central diffusion flame.

The perforated plate burner made of stainless steel that is being displayed has an exterior diameter (D) of 30 mm and a thickness of 3 mm. With a length (L) of 210 mm from the mixing point to the burner tip, the burner duct length results in a partial-premixing ratio of L/D of 7. For the sake of flame stability, a perforated plate is utilized that has 22 holes, 4-mm each, and one central hole with 6-mm diameter for the central diffusion stream. This type of burner is preferred over a large size single-hole burner because it provides better flame stability. Each hole has several recirculation zones downstream, which provide an area where mass and energy transfer from burned to unburned gases is enhanced [36].

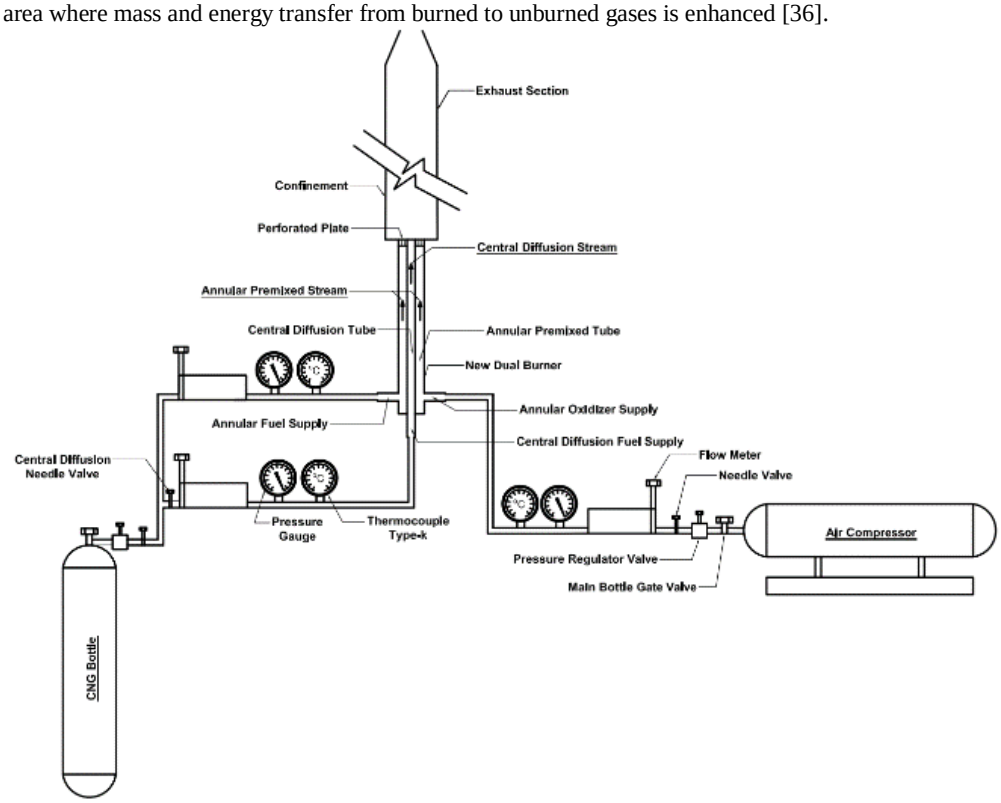

Fig. 1. Test rig flow diagram.

Table 1: Instruments specifications.

Instruments	Specifications			
	Range	Resolution	Accuracy	Manufacture
CNG premixed rotameter	0.47 – 4.7 LPM	0.24 LPM	± 3%	
CNG diffusion rotameter	0.06 – 0.5 LPM	0.02 LPM	± 5%	Dwyer
Air rotameter	1 – 20 LPM	0.5 LPM	± 3%	
Pressure gauge	0 – 1 Bar	0.02 bar	± 2.5%	Simga
Thermo. Type-k	-40 – 1000°c	1 °c	± 1.5%	Autoboss

The resulting primary annular flame is regarded as a somewhat partially-premixed flame since it is neither totally premixed nor purely diffusion, where the secondary central flame is a fully non-premixed CNG flame. To prevent the partially-premixed flammable mixture from exploding in the event of a flashback, three flame arrestors are placed along its route. To ensure contained flame operation, a confinement (a steel cylinder measuring 500 mm in length, 7 mm in thickness, and 150 mm in inner diameter, or Dc) is utilized. The wall effects are negligible since the confinement ratio, $(Dc/D)^2$, is 25 [32]. In order to prevent air from entering into the system, an exhaust section (1 m long and 150 mm in diameter) comes after the confinement.

To avoid air entrainment into the combustion zone, the exhaust section terminates with a cone that is 200 mm long and 40 mm in exit diameter. To provide optical access for taking digital pictures of the flames, a rectangular sight glass that is 70 mm by 250 mm in size and 10 mm thick is placed on the outside of the enclosure and sealed thus preventing leakage.

The visual appearance of the flame under various conditions is captured using a high-resolution digital camera (Canon EOS D750, with a 24.2 Mega pixel resolution). To record the average flame shape, all photographs are taken in a darkened lab

space using night vision mode with a shutter speed of 1/60 s. The frame rate of the camera is 25 frames per second. By contrasting the flame length in the image with a reference length scale, the visual flame length is determined. Additionally documented are the extinction mechanisms (blow-out/blow-off//flash-back).

2.2. Operating conditions

In this study, an experimental examination of the operability limits of an extra-lean dual diffusion/partially-premixed CNG-Air stabilized flames are directed over a perforated plate. The tests were carried out across a wide range of equivalence ratios, and a range of diffusion ratios (the ratio of diffusion fuel volume flow rate to the premixed fuel volume flow rate) from 0 %, 5 %, 10% and 15 %. This work identifies the extinction mechanisms for CNG-Air partially/premixed flames with central CNG diffusion flames. In order to examine the flame characteristics, the study also documents the color, look (inner and outer cones), and perceived flame length. The operability limits are examined throughout the following ranges: flow Reynolds number (from 640 to 1120), diffusion ratios (from 0% to 15%), and equivalence ratios (from 0.09 to 1.33). Airflow is used for purging the system before the annular partially-premixed mixture and central diffusion fuel are added in all tests.

To ascertain the range of equivalence ratios required for flame operability at a diffusion ratio of zero percent, the first set of tests was conducted. The second set of research examined the operability and flammability limits of CNG-air combustion at different diffusion ratios of 5, 10, and 15% with a 0% diffusion ratio. The air Reynolds number ranged from 640 to 1120 during the studies.

The following are the definitions of the diffusion ratio, Reynolds number, and equivalence ratio:

$$\Phi = \frac{(\frac{\dot{m}a}{\dot{m}f})stoichiometric}{(\frac{\dot{m}a}{\dot{m}f})actual}$$

$$Re_{oxidizer} = \frac{4 * \dot{m_{air}}}{\pi * D * \mu_{air}}$$

$$Diff.\ Ratio\ \% = \frac{\dot{V}\ cng_{\ central\ diffusion}}{\dot{V}\ cng_{\ premixed}}$$

3. Computational model setup

3.1. Numerical model

The configuration utilized for this investigation is represented by the chosen numerical model, as shown in Fig. 2. For a premixed combination, two circular ports (3 mm high and 4 mm inner diameter) discharge a uniform stream of mixed CNG-Air upward into the domain at a velocity of U_{In} = 1 m/s, which corresponds to Re of 835. To create 5%, 10%, and 15% diffusion flames, a second, uniform stream of pure CNG is released from the 6 mm central hole at varying speeds. The open border is subject to pressure outlet boundary conditions, whereas the axis is subject to a symmetric boundary condition. In this study, a non-slip conductive burner is taken into consideration. The calculation total domain is 75 mm by 500 mm. In the x and r axes, stretched and structured meshes are applied; a very tiny, fine grid is positioned close to the solid burner tube, and a larger grid size is positioned toward the far outer bounds, totaling 237805 mesh cells.

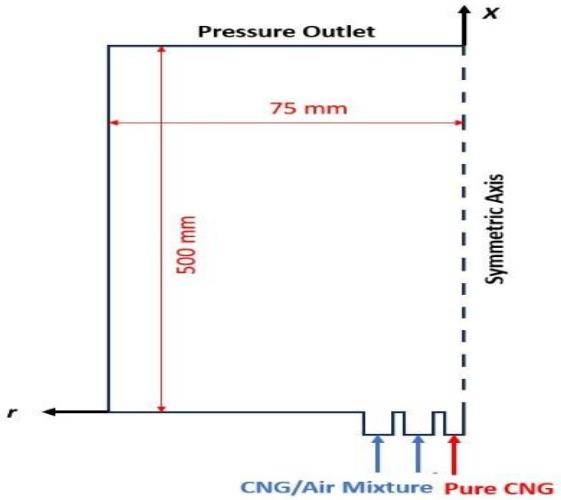

Fig. 2. Adopted numerical model

Steady, axisymmetric, and two-dimensional heat and mass transport equations are solved numerically using multi-step chemical reaction mechanisms.

$$\nabla . (\rho\vec{u})=0 \quad (1)$$

$$\nabla . (\rho\vec{u}\vec{u})= \nabla P + \nabla (\mu\nabla\vec{u}) + \rho g_x \quad (2)$$

$$\nabla . (\rho\vec{u}T)=\frac{1}{Cp} \nabla. (\lambda\nabla T) - \frac{1}{Cp}\sum_{i=1}^{N} hi\omega i \quad (3)$$

$$\nabla . (\rho\vec{u}Yi)=\nabla. [\rho Di \nabla Yi + \rho D_i^t \nabla (\ln T)]+\omega i \quad (4)$$

$$P= \rho R_o T \sum_{i=1}^{N} \frac{Yi}{Mi} \quad (5)$$

The solution of these governing equations was done by employing ANSYS FLUENT 17.0 CFD package [37]. The chemistry of combustion is modeled by using Deutschmann reaction mechanism.

3.2. Chemical Kinetics model

This study uses the TCI model (no turbulence-chemistry interaction). Without attempting to explicitly account for the effects of turbulent fluctuations on the source term computations, kinetics of finite rate are integrated by assessing the chemical source terms using expressions of general reaction rate. For laminar flows, if the formulation is precise, as in the present study, this approach is recommended.

According to this model, the net source of the chemical species i resulting from the reaction r is determined by adding up the sources of the reaction across all of the NR processes in which the species is involved:

$$R_i=M_{w,i} \sum_{r=1}^{Nr} \hat{R}_{i,r} \quad (6)$$

Where $M_{w,i}$ is the molecular weight of species i and $\hat{R}_{i,r}$ is the molar rate of creation/destruction of species *i* in reaction *r*.

The molar rate of creation/destruction of species *i* in reaction *r* is given by

$$\hat{R}_{i,r}= \Gamma (v''_{i,r}-v'_{i,r}) (k_{f,r} \prod_{j=1}^{N}[C_{j,r}] \eta'_{j,r} - k_{b,r} \prod_{j=1}^{N}[C_{j,r}] v''_{j,r}) \quad (7)$$

Where:

$C_{j,r}$= species *j* molar concentration in the reaction *r*

$\eta'_{j,r}$ = reactant species *j* rate exponent in reaction *r*

$\eta''_{j,r}$= product species *j* rate exponent in reaction *r*

$v'_{i,r}$= reactant *i* stoichiometric coefficient in reaction *r*

$v''_{i,r}$= product *i* stoichiometric coefficient in reaction *r*

$k_{f,r}$= reaction *r* forward rate constant

$k_{b,r}$= reaction *r* backward rate constant

3.3. Chemical reaction mechanism

Reaction mechanisms for premixed combustion, such as backward reaction, third body efficiency, and coverage-dependent reaction, are imported into CHEMKIN to describe volumetric reactions. Deutschmann [38] developed this simple heterogeneous technique to forecast the combustion process. The detailed mechanism of burning is shown by 17 gas-phase species (CH_4, CH_3, CH_2, CH, CH_2O, HCO, CO_2, CO, H_2, H, O_2, O, OH, HO_2, H_2O_2, H_2O, and N_2).

4. Results and discussion

4.1. Operability limits

Fig.3. demonstrates the relationship between the equivalence ratio and the air Reynolds number at 0%, 5%, 10% and 15% diffusion ratios to observe and plot the operability map for the burner considered. It is well known that the operability limits decreases and becomes narrowest as the Reynolds number increases as shown in the Fig. [39-42]. Investigating the lower Reynolds number at which the burner operates in a stable mode without flashback has significance in this case, nevertheless. Flashback zone occurs at lower Reynolds number (lower than Re = 640) because in this range the flow velocity is lower than the burning velocity. The results reveal that the operability curve in terms of the equivalence ratio, φ, becomes wider with increase the diffusion ratio. The maximum upper operability limit (at average value of Re = 835) was φ = 1.33 achieved at 15% diffusion. However, on the lean side, the extra-lean diffusion/partially-premixed burner has an operability range that extends into extra lean conditions with recorded φ = 0.04 at a 5% diffusion ratio at the same Re = 835.

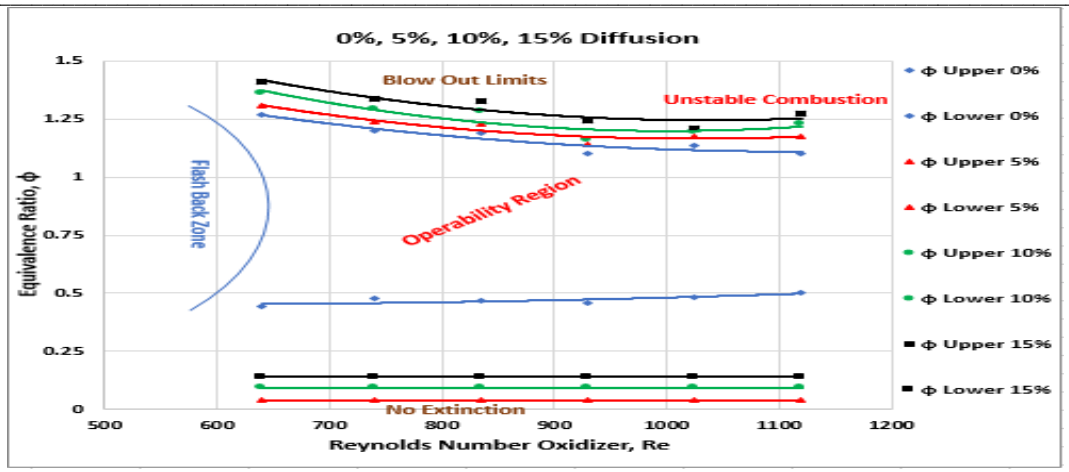

Fig. 3. Impact of diffusion ratios on the operability curve for CNG-Air flames over the range of oxidizer Reynolds number from 640 to 1120

4.2. Flammability limits

Figure 4 shows how the fuel flow rate and the oxidizer Reynolds number relate to one another for various diffusion ratios. The Reynolds number is known to increase with the fuel mass flow rate, as shown in Fig. [39-42]. Flammability limitations are established by adjusting the air mass flow rate and equivalency ratio to a particular stable value. The diffusion ratio that has to be measured is then opened and set. The fuel mass flow rate increases gradually until the upper flammability limits are reached while maintaining a constant oxidizer (air) mass flow rate and a particular diffusion ratio for each case of 0, 5, 10, and 15%, respectively. However, in this case, it is crucial to examine the values of extra-lean fuel flow rates at lower flammability limitations. This pattern of behavior is caused by the general trend in CNG-air combustion that diffusion flames are more stable than premixed flames. The central diffusion flame significantly alters the known lower flammability limits, which have no lower extinction over all diffusion ratios, but the upper side extinction mechanisms are caused by blow-out, this shows that the flame is blowing out because its speed is less than the flow speed of the flammable mixture. The maximum upper flammability limit (at average value of Re = 835) was Mf = 0.101 kg/h achieved at 15% diffusion ratio, where the minimum lower flammability limit has been carried out at 5% diffusion ratio with Mf = 0.003 kg/h and at the same Re = 835.

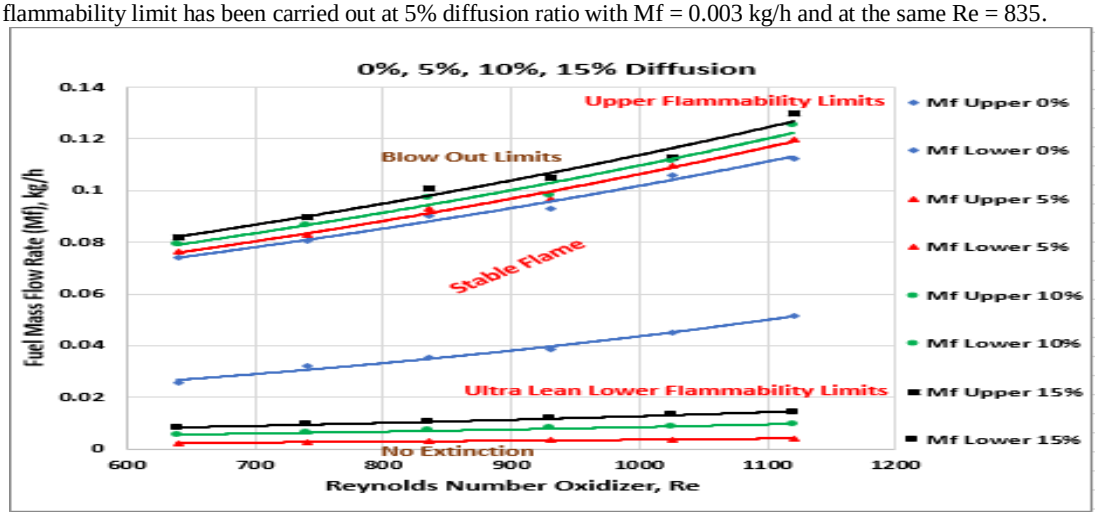

Fig. 4. Impact of diffusion ratios on the flammability limits for CNG-Air flames over the range of oxidizer Reynolds number from 640 to 1120

4.3. Visual flame characterization

A professional camera was used to take pictures of flames in order to investigate how various elements affected the visual flame length, appearance, and color. The images in the set, which were taken at various equivalence ratios while maintaining a constant oxidizer Reynolds number of roughly 835, demonstrate the visual appearance of the flame at 0,5,10 and 15% diffusion ratio.

4.3.1Flame visualization at diffusion ratio 0,5,10 and 15% and Reynolds number = 835

Ten different flames were carefully selected for each diffusion ratio in order to track the visual appearance of the flames and examine how equivalence ratios affect the visual characterization of these flames inside the stable combustion zone. From

the lower extinction limit at φ = 0.47 to the upper extinction limit at 1.19, the visual flame appearance and color of a flame with a 0% diffusion ratio are displayed in Fig. 5 (1st row). In the flame, a larger outer cone surrounds smaller inner cones with higher equivalence ratios. The inner cones, which were the first step in the burning process, are where the gas is burned. As the fuel flow rate is decreased, the flame length gradually diminishes and the outer cone eventually vanishes.

Fig. 5 (2nd, 3rd, and 4th rows) shows the appearance of the flame at 5, 10, and 15% central diffusion flames on a partially-premixed burner. For a 5% diffusion ratio, the visual flame appearance is between φ = 0.04 and 1.23; for a 10% diffusion ratio, it is between φ = 0.09 and 1.28; and for a 15% diffusion ratio, it is between φ = 0.14 and 1.33. When a central diffusion flame with a different ratio of 5% was added, the burner's lower limit of operation decreased to 91.5% at φ = 0.04 compared to a 0% diffusion ratio, creating a new target of operation at a very low equivalence ratio. For these cases, the flame is composed of an extended and yellow central diffusion cone, while the outer annular partially-premixed cone become less bright and visible due to the presence of the bright yellow central diffusion flame cone as well as the small inner blue cones are surrounded by the outer cone. The flame overall shape and size gradually decreases as the fuel flow rate is reduced, and the outer cone gradually fades as the inner cones combine to form thinner, weaker cones. However, there would be no lower blow-off occur due to the existence of the yellow central diffusion flame with sufficient oxygen.

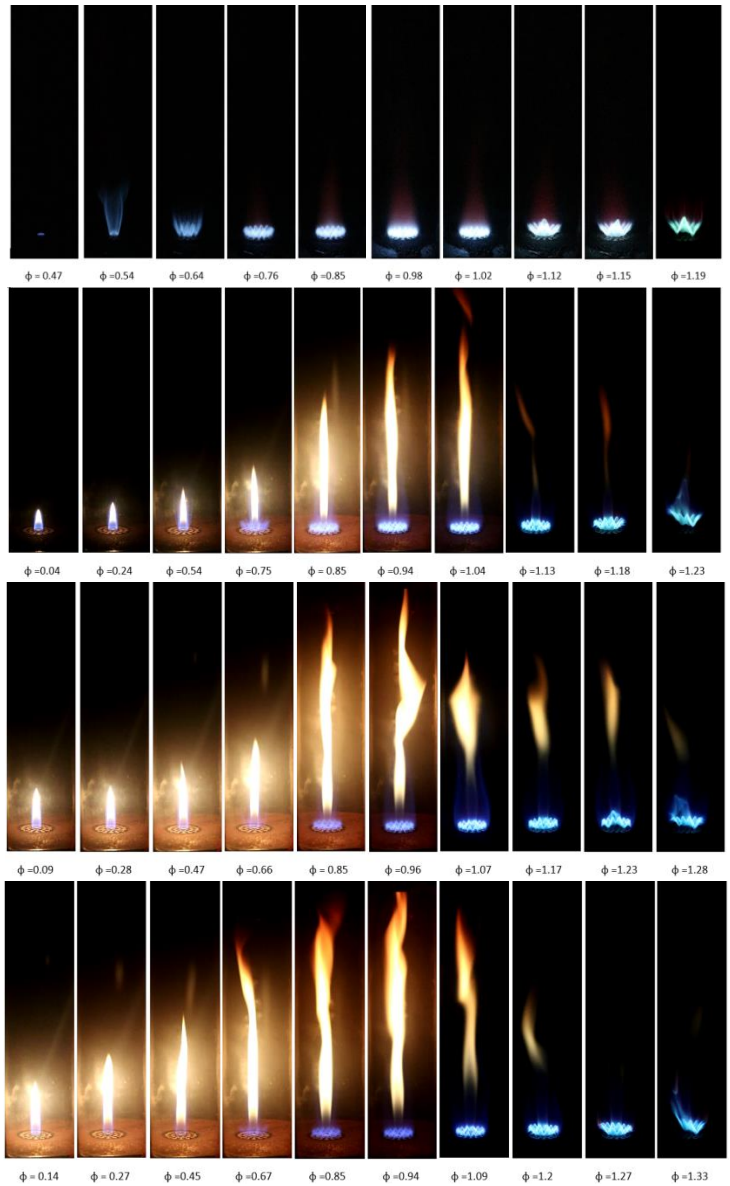

Fig. 5. Effect of equivalence ratio, on visual flame appearance at Re=835, on the inner and outer cone structure of the CNG-Air flames at diffusion ratio 0% (1st row), 5% (2nd raw), of 10% (3rd raw) and 15% (4th raw).

To examine the variation in flame length between lower and upper limits at fixed Re = 835, Fig. 6 shows the visible flame length throughout a range of φ at various diffusion ratios of 0, 5, 10, and 15%, respectively. By comparing the flame length in the picture to a reference length scale in the experimental apparatus, the flame length was determined. This reference length scale, which shows the true length of the flame in the taken image, is just a ruler positioned normal to the burner plate. From the burner plate to the flame shape tip, the flame length was determined. Before the upper extinction limit occurs, the digital photos demonstrate that the total visual flame length and size increased gradually as the equivalence ratio increased and subsequently reduced as the equivalence ratio continued to increase. At 15% diffusion ratio, the greatest flame length was observed to be 29.13 cm at φ = 0.94, which was 246.8% larger than at 0% diffusion ratio at the same equivalence ratio of 0.94. It is observed that as the diffusion ratios increased, the overall flame length through the extinction process increased from lower to upper limits.

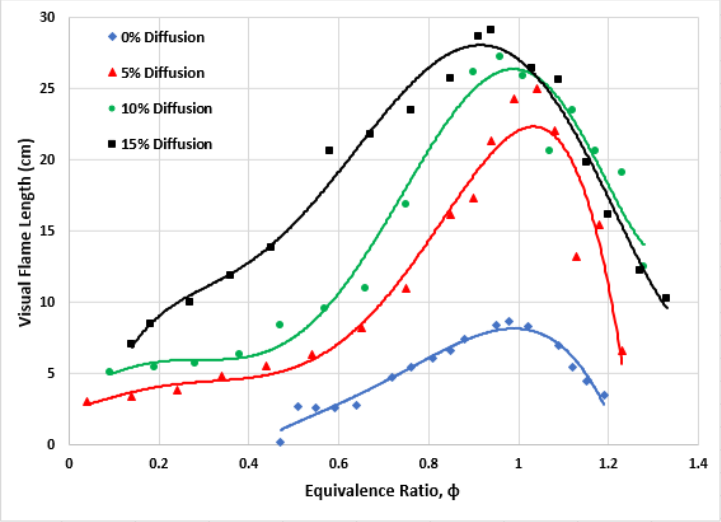

Fig. 6. Visual flame length over the range of equivalence ratio from 0.04 to 1.33 at different diffusion ratios

The variation of visual flame length at different diffusion ratios namely 0, 5, 10 and 15%, respectively was shown in Fig. 7. The visual flame length was obtained at φ = 0.85 and Re = 835. The Fig. shows that visible flame length is elongated by increasing of the diffusion ratio, this is due to the high ejecting velocity of CNG central diffusion flame. The maximum flame length was achieved at 15% diffusion ratio and recorded 25.75 cm. The flame length at 15% diffusion ratio remain constant for 10% diffusion ratio, while recorded an increase of 59.2% compared to 5% diffusion ratio and an increase of 290.15% compared to 0% diffusion ratio.

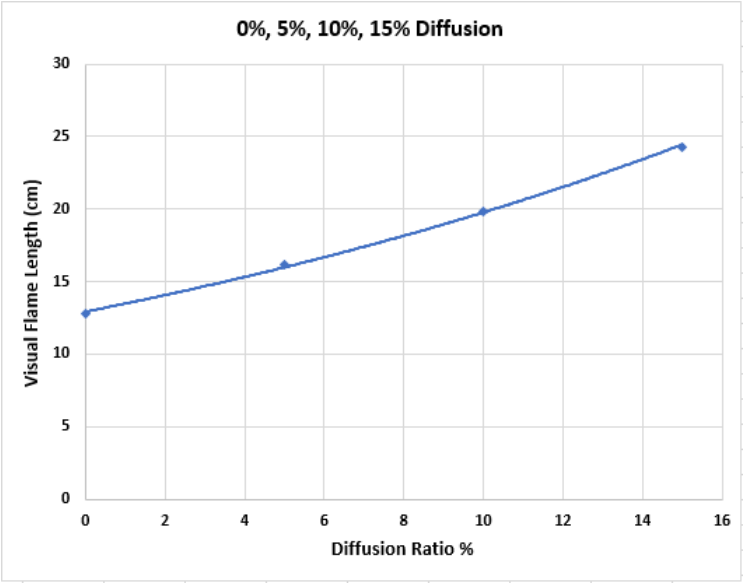

Fig. 7. Visual flame length over the range of diffusion ratio from 0 to 15%

4.4. Thermal structure of CNG-Air flame under different diffusion ratios

A 1 m/s (Re = 835) CNG-Air mixture was released from exterior holes to examine the impact of diffusion flames under various diffusion ratios on flame thermal structure. From the central hole, pure CNG was released to create diffusion flames at 5, 10, and 15%. The two-dimensional temperature contours of the calculated flame at φ = 0.85 are displayed in Fig. 8.

The findings demonstrate that low-temperature fuel ejecting from the central hole caused the maximum flame temperature to drop as the diffusion ratio increased, particularly at the axial axis. The ejecting diffusion fuel flow into the reaction zone just above the burner tip has increased, causing the temperature to drop. This decreases the reactivity and transforms the almost stoichiometric mixture (φ = 0.85) into a rich mixture. Furthermore, contours show that varying diffusion flame ratios have a temperature impact on the premixed flame outer cone. The premixed flame outer cone gradually faded away and created two small triangles on either side of the core diffusion flame as the central diffusion ratio increased, decreasing the outer cone overall shape.

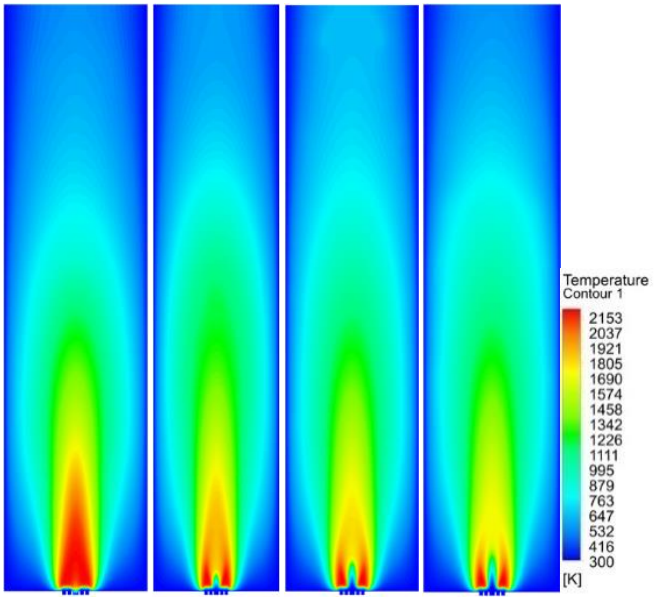

Fig. 8. Two-dimensional temperature contours over the range of diffusion ratio from 0 to 15% at φ = 85 and Re = 835

The corresponding one-dimensional temperature distribution along the x-axis (axial axis) for the different diffusion ratios is displayed in Fig. 9. The Fig. shows a sudden change in the flame profile right after the burner tip (at x = 0 mm). The chemical reaction zone moved upward and away from the burner tip as the diffusion ratio rose to 5, 10, and 15%, while the 0% diffusion burner showed an increasing temperature gradient. The maximum flame temperature of 2193.29 K was reached at a 0% diffusion ratio at an axial distance of 0.033 meters from the burner tip. A 15% diffusion ratio resulted in a maximum flame temperature of 1713.73 K at an axial distance of 0.06 meters from the burner tip, representing a relative drop of 21.86% in comparison to a 0% diffusion ratio.

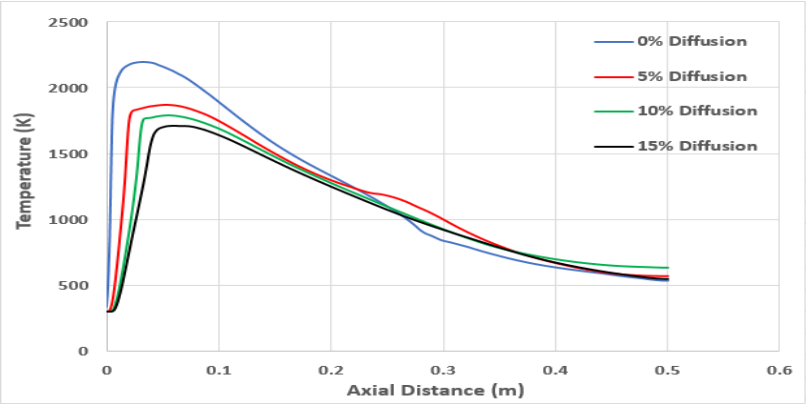

Fig. 9. Computational axial temperature over the range of diffusion ratio from 0 to 15% at φ = 85 and Re = 835

4.5. Detailed flame chemical structure under different diffusion ratios

The computed species mass fraction are shown to give an idea of how the center diffusion ratios affect the chemical flame structure. The combustion model is based on the Deutschmann chemical reaction process. Axially along the flame centerline, the mass fraction of the primary principal species (CO_2, H_2O, O_2, and CO) were calculated at the same time.

4.5.1Major species mass fraction distributions

A 1 m/sec CNG-Air premixed mixture with three distinct diffusion flames (namely, 5, 10, and 15% diffusion ratios) was created in order to numerically investigate the impacts of diffusion ratio on the flame chemical structure. Temperature and main species in the axial direction were calculated computationally using Deutschmann's chemical reaction mechanisms [33].

Fig. 10, Fig. 11, Fig. 12, and Fig. 13 show the calculated temperature and the principal species mass fraction (CO_2, H_2O, O_2, and CO) with axial distance.

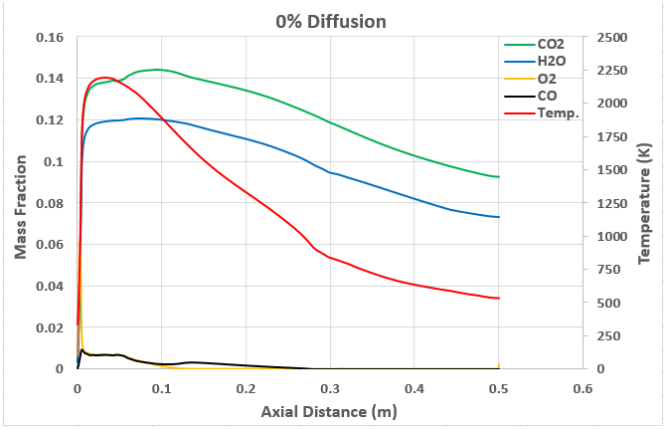

Fig. 10. Computational axial temperature major species mass fraction at diffusion ratio 0%, φ = 85 and Re = 835

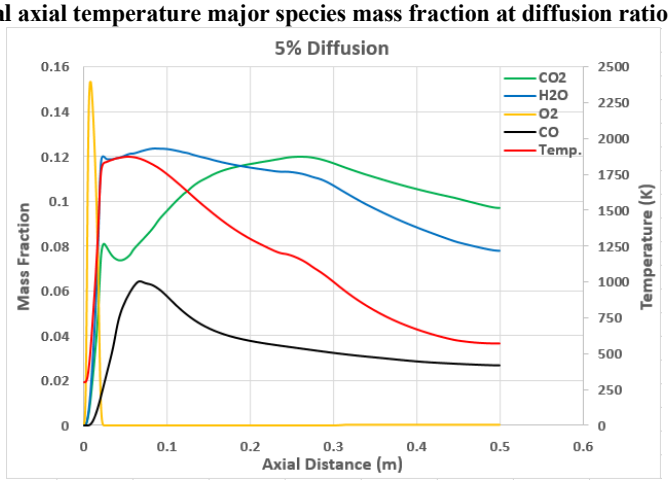

Fig. 11. Computational axial temperature major species at diffusion ratio 5%, φ = 85 and Re = 835

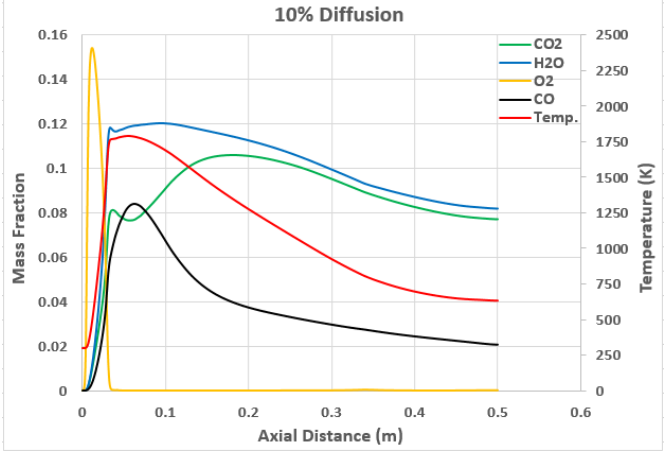

Fig. 12. Computational axial temperature major species mass fraction at diffusion ratio 10%, φ = 85 and Re = 835

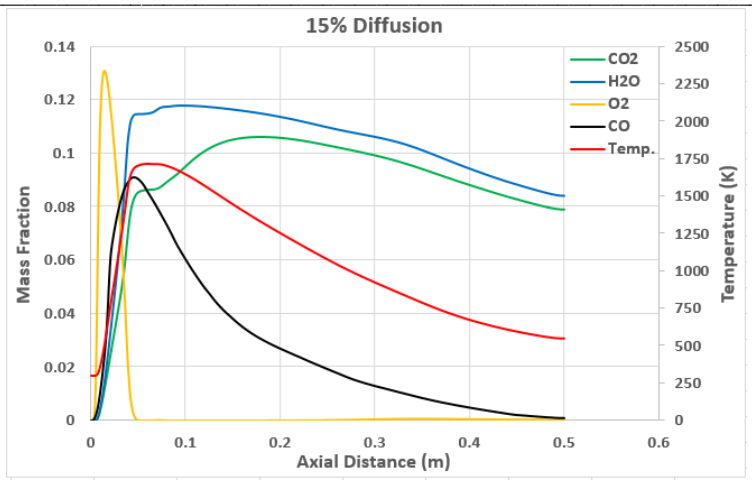

Fig. 13. Computational axial temperature major species mass fraction at diffusion ratio 15%, φ = 85 and Re = 835

With the exception of the highest axial temperature, there were no discernible variations in the H_2O and O2 main species mass percentage of the 5%, 10%, and 15% computed flames. In contrast, the CO concentration in the 0% diffusion flame was, as predicted, lower than in diffusion environments. The output results are shown in this section.

The chemical reaction zone was seen immediately after the burner tip at diffusion ratio = 0% (Fig. 10), with the highest temperature recorded at 0.033 m being 2193.29 K. The highest CO2 and CO concentrations were measured to be 0.144281 and 0.009225, respectively. As anticipated, Fig. 11 (at diffusion ratio = 5%) shows an increase in CO concentration and a decrease in maximum axial temperature and CO2 concentration. Diffusion flame entraining from the center hole, which lowers the chemical reactivity, is the cause of the noticeable variations in flame thermal and chemical structures. The clams are reassured that the reaction zone moved upward and away from the burner tip because the maximum axial temperature in this instance was lowered to 1869.71 K at 0.053 m. Additionally, it was discovered that the highest CO_2 and CO concentrations were 0.119899 and 0.090796, respectively. As seen in Figs. 12 and 13, such tendencies continue at DP = 10% and DP = 15%, where the calculated maximum axial temperature was 1789.43 K and 1713.73 K, respectively. It was discovered that the maximum CO concentrations for diffusion flames at 10% and 15% were, respectively, 0.084172 and 0.064274.

4.6. Comparative analysis

Table 2 provides a thorough evaluation of how the center diffusion flame affects the visual flame characterization and combustion characteristics of CNG-Air flames stabilized over an extra-lean dual diffusion/partially-premixed burner.

The impact of diffusion flame ratio on the numerical maximum axial temperature, CO, and CO_2 mass fraction is also shown in Table 2. A constant oxidizer Reynolds number of about 835 was used for all comparison data. In order to simulate an 835 Re partially-premixed flame and four distinct diffusion flames ejected from the central hole, a 1 m/sec partially-premixed mixture flame was calculated for the numerical model. The effect of adding a central diffusion flame to the annular partially-premixed flame at ratios of 5, 10, and 15%, respectively, was examined in the comparison study, and the outcomes were compared with a diffusion ratio of 0%.

In Table 2, the detailed numerical measured and computed data illustrated the relative change compared to a 0% diffusion ratio for the influential parameters namely; upper and lower equivalence ratio, upper and lower fuel mass flow rate, flame length, maximum computed axial flame temperature, CO_2, and CO mass fraction. ((+) indicates an increase and (-) decrease).

The comprehensive comparisons for the measured data were obtained at φ = 0.85 and Re = 835. The maximum upper equivalence ratio was achieved at 15%, where the minimum lower equivalence ratio was 5%. The maximum upper and minimum lower fuel mass flow rates were recorded at 15% and 5%, respectively, while the maximum flame length was recorded at 15%. On the other hand, the comprehensive comparisons for the computed data were achieved with a minimum axial flame temperature at a 15% diffusion ratio, while the mass fraction of CO_2 was recorded as a minimum decrease at a 5% diffusion ratio, and CO was recorded as a maximum increase at 10 and 15% diffusion ratios.

Table 2: Comparison of combustion characteristics, visual flame length, chemical and thermal structure compared to 0% diffusion ratio at φ = 0.85 and Re=835.

Relative change, %	Diffusion ratio		
	5%	10%	15%
Upper equivalence ratio	+3.3%	+7.8%	+11.7%
Lower equivalence ratio	-91.5%	-80.9%	-70.2%
Upper fuel mass flow rate	+3.3%	+7.9%	+11.8%
Lower fuel mass flow rate	-91.6%	-80%	-70%
Visual flame length	+145.1%	+290.1%	+290.1%
Axial flame temperature	-14.75%	-18.41	-21.86
Axial CO2 mass fraction	-16.89%	-26.57%	-26.59%
Axial CO mass fraction	+884.2%	+812.3%	+596.7%

5. Conclusions

A new dual-stream burner that offers a comprehensive chemical analysis of CNG-Air combustion has been used to experimentally investigate the stability and combustion chemical properties of dual diffusion/partially premixed flames. In addition to directly affecting combustion efficiency and pollutant concentrations, the effect of flame stability on emission is an essential factor in enhancing the chemical analysis of combustion.

Using a skeleton chemical reaction mechanism, a numerical research is conducted to clarify the thermal and chemical structures created in the dual-stream burner. Additionally, temperature and concentrations of the main species (CO_2, H_2O, O_2, and CO) have been measured.

Summary of the main conclusions are stated below:

- Effect of the diffusion ratio on the operability map: The use of different diffusion ratios leads to a wider flame operability map through the upper and lower extinction limits, improving flame stability, reducing fuel consumption, and hence achieving clean combustion. However, operating at very low Reynolds number causes flashback due to the lower ejecting velocity.
- Effect of the diffusion ratio on the visual flame appearance and length: Before the upper extinction limit occurs, the digital photos demonstrated that the total visible flame length and size increased gradually as the equivalence ratio increased and then reduced after stoichiometric. The increase of the diffusion ratio caused a significant increase in flame shape, size, and length.
- Effect of diffusion ratio on thermal and chemical structure of the flame: Numerical investigation showed that the maximum axial flame temperature decreased and the reaction zone moved up away from the burner due to low-temperature fuel ejecting from the central hole and poor reactivity caused by the central diffusion flame, which will minimize the formation of NOx. The H_2O and O_2 main species mass fractions of the 5%, 10%, and 15% computed flames did not differ significantly, according to the computational results. However, as the diffusion ratio grew, the CO2 was significantly reduced. Nevertheless, the CO concentration rose as the central diffusion ratio increased.

6. References

[1] Medhat Ahmed Nemitallah, Sherif S. Rashwan, Ibrahimm B. Mansir, Ahmed A. Abdelhafez, and Mohamed A. M. Habib. Review of novel combustion techniques for clean power production in gas turbines: review. Energy & Fuels 2018, 32, 2, 979–1004.
[2] Muhammad Nauman, Jianfeng Pan, Yu Wang, Feiyang Li, Abiodun Oluwaleke Ojo, Ali Raza. A review of recent advancements in micro combustion techniques to enhance flame stability and fuel residence time: review. International Journal of Hydrogen Energy 2024, 49, A, 1165-1193.
[3] Medhat A. Nemitallah, Ahmed A. Abdelhafez, Asif Ali, Ibrahim Mansir, Mohamed A. Habib. Frontiers in combustion techniques and burner designs for emissions control and CO2 capture: review. International Journal of Energy Research 2019;1–33.
[4] Kashir, B.; Tabejamaat, S.; Jalalatian, N. International journal of hydrogen energy 2015, 40, 6243–6258.
[5] Habib, M. A.; Nemitallah, M. A.; Ahmed, P.; Sharqawy, M. H.; Badr, H. M.; Muhammad, I.; Yaqub, M. Energy 2015, 86, 105–114.
[6] Yu, B.; Lee, S.; Lee, C. E. Energy 2015, 91, 119–127.
[7] Gao, X.; Duan, F.; Lim, S. C.; Yip, M. S. Energy 2013, 59, 559–569.
[8] Li, Y. H.; Chen, G.B.; Lin, Y. C.; Chao, Y. C. Energy 2015, 89, 845–857.

[9] Altay, H. M.; Hudgins, D. E.; Speth, R. L.; Annaswamy, A. M.; Ghoniem, A. F. Combustion and flame 2010, 157, 686–700.
[10] Ghoniem, A. F.; Park, S.; Wachsman, A.; Annaswamy, A.; Wee, D.; Altay, H. M. Proceedings of the combustion institute 2005, 30, 1783–1790.
[11] Lee, K.; Kim, H.; Park, P.; Yang, S.; Ko, Y. Fuel 2013, 106, 682–689.
[12] S. Taamallah, K. Vogiatzaki, F.M. Alzahrani, E.M.A. Mokheimer, M.A. Habib, A.F. Ghoniem. Fuel flexibility, stability and emissions in premixed hydrogen-rich gas turbine combustion: Technology, fundamentals, and numerical simulations. Applied Energy 2015, 154, 1020-1047.
[13] Tim Lieuwen, Vince McDonell, Eric Petersen, Domenic Santavicca. Fuel Flexibility Influences on Premixed Combustor Blow-out , Flashback, Autoignition, and Stability. J. Eng. Gas Turbines Power. 2008, 130(1): 011506.
[14] Sherif S. Rashwan, Medhat Ahmed Nemitallah, and Mohamed A. Habib. Review on premixed combustion technology: Stability, emission control, applications and numerical case study: review. Energy & Fuels 2016, 30, 12, 9981–10014.
[15] Abdul-Wahab SA, Charabi Y, Al-Maamari R, Al-Rawas GA, Gastli A, Chan K. CO2 greenhouse emissions in Oman over the last forty-two years: review. Renew Sustain Energy Rev 2015;52:1702–12.
[16] R. M. Mohamed, H. M. A. Hashish, H. A. Abdel-Samad, M. E. Awad, and G. A. Kadry, "A Competent, Humble Cost Catalyst from Biowaste: High Performance and Combustion Characteristics of Alternative Diesel Fuel," Egypt. J. Chem., vol. 65, no. 13, pp. 265–277, Dec. 2022, doi: 10.21608/EJCHEM.2022.117718.5306.
[17] H. M. M. Mustafa, R. M. Kamal, and M. R.M., "Enhancing and optimization of green hydrogen mixtures in natural gas to optimize transportation, power, and Economy," Egypt. J. Chem., vol. 67, no. 11, pp. 491–501, Nov. 2024, doi: 10.21608/ejchem.2024.279356.9513.
[18] Mustafa, H. M. M., Kamal, R. M., & Mohamed, R. M. (2024). The optimal proportion for blending hydrogen with natural gas to facilitate its utilization and transportation through the national gas transportation. Egyptian Journal of Chemistry, 67(13), 559–566.
[19] Gad, M. S., Hashish, H. M. A., Hussein, A. K., Abdulkader, R., & Nasef, M. H. (2024). Effect of different configurations of hybrid nano additives blended with biodiesel on CI engine performance and emissions. Scientific Reports, 14(1), 19528.
[20] Ibrahim, S. M. A., Abed, K. A., Gad, M. S., & Mustafa, H. M. M. (2024). The performance of a developed diesel vehicle to run on WCO biodiesel at variable speeds and loads | Osiągi opracowanego pojazdu z silnikiem Diesla przystosowanego do zasilania biodieslem WCO przy zmiennych prędkościach i obciążeniach. Polityka Energetyczna, 27(2), 105–127.
[21] Ibrahim, S. M. A., Abed, K. A., Gad, M. S., & Hashish, H. M. A. (2024). Performance and emissions of a diesel engine burning blends of Jatropha and waste cooking oil biodiesel. Proceedings of the Institution of Mechanical Engineers, Part C: Journal of Mechanical Engineering Science, 238(4), 1157–1169.
[22] Khalaf, M., Xuan, T., Abdel-Fadeel, W. A., Abdelhady, S., & Esmail, M. F. C. (2024). A comparative study of diesel engine fueled by Jatropha and Castor biodiesel: Performance, emissions, and sustainability assessment. Process Safety and Environmental Protection, 188, 453–466.
[23] Ibrahim, S. M. A., Abed, K. A., Gad, M. S., & Hashish, H. M. A. (2020). Experimental study on the effect of preheated Egyptian Jatropha oil and biodiesel on the performance and emissions of a diesel engine. International Journal of Mechanical and Mechatronics Engineering, 20(1), 59–69.
[24] R. M. Mohamed, H. M. M. Mustafa, A. M. Shoaib, A. A. Afify, G. K. Hassan, and W. M. Shehata, "Maximization of Biodiesel production from oil that produced during salmon smoking process with high amount of omega-3 by using homogenous catalyst," Environ. Sci. Pollut. Res. 2024, pp. 1–21, Oct. 2024, doi: 10.1007/S11356-024-35254-X.
[25] Jaramillo P, Griffin W Michael, Matthews HS. Comparative life-cycle air emissions of coal, domestic natural gas, LNG and SNG for electricity generation. Environ Sci Technol 2007;41:6290–6.
[26] Taamallah S, Vogiatzaki K, Ghoniem A, Alzahrani F, Mokheimer E, Habib MA. Fuel flexibility, stability and emissions in premixed hydrogen-rish combustion: technology, fundamentals and numerical simulations. Appl Energy 2015;154:1020–47.
[27] Barlow RS, Karpetis AN, Frank JH. Scalar profiles and NO formation in laminar opposed-flow partially premixed methane/air flames. Combust Flame 2001;127:2102–18.
[28] Hongshe X, Suresh KA. NOx emissions in n-heptane/air partially premixed flames. Combust Flame 2003;132:723–41.
[29] Seiser R, Trutte L, Seshadri K. Extinction of partially premixed flames. Proc Combust Inst 2002;29:1551–7.
[30] Sayangdev N, Aggarwal SA. Fuel effect on NOx emissions in partially premixed flames. Combust Flame 2004;139:90–105.
[31] Tyliszczak A, Boguslawski A, Nowak D. Numerical simulations of combustion process in a gas turbine with a single and multi-point fuel injection system. Appl Energy 2016;174:153–65.
[32] Nemitallah MA, Habib MA. Experimental and numerical investigations of an at mospheric diffusion oxy-combustion flame in a gas turbine model combustor. Appl Energy 2013;111:401–15.
[33] Taamallah S, Vogiatzaki K, Alzahrani FM, Mokheimer EMA, Habib MA, Ghoniem AF. Fuel flexibility, stability and emissions in premixed hydrogen-rich gas turbine combustion: technology, fundamentals, and numerical simulations. Appl Energy 2015;154:1020–47.
[34] Park J, Minamoto Y, Shimura M, Tanahashi M. Effects of hydrogen enrichment on CH4/Air turbulent swirling premixed flames in a cuboid combustor. Int J Hydrogen Energy 2020;45:9039e51.
[35] Guo S, Wang J, Zhang W, Zhang M, Huang Z. Effect of hydrogen enrichment on swirl/bluff-body lean premixed f lame stabilization. Int J Hydrogen Energy 2020;45:10906e19.
[36] Ditaranto M, Hals Jorgen. Combustion instabilities in sudden expansion oxyfuel flames. Combust Flame 2006;146:493–512.

[37] http://www.ansys.com/Products/Fluids/ANSYS-Fluent.
[38] O. Deutschmann, Interactions Between Transport and Chemistry in Catalytic Reactors.Habilitationschrift, Universität Heidelberg, 2001.
[39] Tim Lieuwen, Vince McDonell, Eric Petersen, Domenic Santavicca. Fuel Flexibility Influences on Premixed Combustor Blowout, Flashback, Autoignition, and Stability. J. Eng. Gas Turbines Power. 2008, 130(1): 011506.
[40] Michele Capurro. Development of a Design Tool for Modern Gas Turbine Combustors and Commissioning of a Gas Turbine Combustion Research Laboratory: thesis. Carleton University Engineering, Environmental Science 2008, https://api.semanticscholar.org/CorpusID:115679885 .
[41] Vince McDonell. Lean Combustion Technology and Control, (Second Edition): book. Academic Press. 2016, 147-201, IV. https://doi.org/10.1016/B978-0-12-804557-2.00005-5 .
[42] Arthur H. Lefebvre, Dilip R. Ballal. Gas Turbine Combustion Alternative Fuels and Emissions, (Third Edition): book. Taylor & Francis Group, LLC. 2010, 121-160,IV. https://doi.org/10.1201/9781420086058 .